Title: Formation of stoichiometric and non-stoichiometric ionic liquid and cocrystal multicomponent phases of lidocaine with azelaic acid by changing counterion ratios

Author: Julija Zotova, Żaneta Wojnarowska, Brendan Twamley, Lidia Tajber

UNIWERSYTET ŚLĄSKI W KATOWICACH   Biblioteka Uniwersytetu Śląskiego   Ministerstwo Nauki i Szkolnictwa Wyższego

Journal Pre-proofs

Formation of stoichiometric and non-stoichiometric ionic liquid and cocrystal multicomponent phases of lidocaine with azelaic acid by changing counterion ratios

Julija Zotova, Zaneta Wojnarowska, Brendan Twamley, Lidia Tajber

Please cite this article as: J. Zotova, Z. Wojnarowska, B. Twamley, L. Tajber, Formation of stoichiometric and non-stoichiometric ionic liquid and cocrystal multicomponent phases of lidocaine with azelaic acid by changing counterion ratios, *Journal of Molecular Liquids* (2021), doi: https://doi.org/10.1016/j.molliq.2021.117737
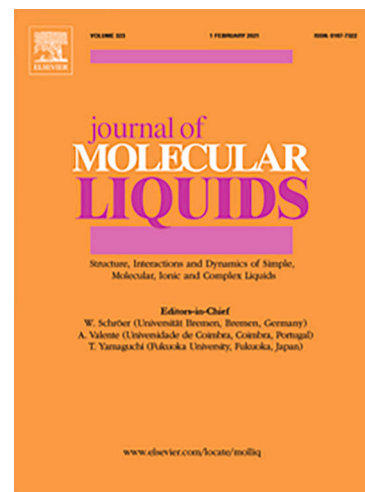
1 **Formation of stoichiometric and non-stoichiometric ionic liquid and cocrystal multicomponent**

2 **phases of lidocaine with azelaic acid by changing counterion ratios**

3 **Authors:**

4 *Julija Zotova[1]; Zaneta Wojnarowska[2]; Brendan Twamley[3]; Lidia Tajber[1*]*

5 **Affiliations:**

6 [1] School of Pharmacy and Pharmaceutical Sciences, Trinity College Dublin, College Green, Dublin 2,

7 Ireland

8 [2] Institute of Physics, University of Silesia, SMCEBI, 75 Pulku Piechoty 1A, 41-500 Chorzow, Poland

9 [3] School of Chemistry, Trinity College Dublin, College Green, Dublin 2, Ireland

10 * Corresponding author, Lidia Tajber, School of Pharmacy and Pharmaceutical Sciences, Trinity College

11 Dublin, College Green, Dublin 2, Ireland. Tel: +35318962787. Email: ltajber@tcd.ie

12

13 **Abstract**

14 Tuning of physicochemical properties of ionic liquids and crystalline materials is a challenge that opens

15 up unlimited possibilities for expanding applications and controlling biological activity of

16 pharmaceutical multicomponent phases incorporating active pharmaceutical ingredients (APIs) with

17 counterions or coformers. In this work we have investigated the effect of changing lidocaine (LID) and

18 azelaic acid (AZE) ratios on the physicochemical properties of their corresponding multicomponent

19 systems using a thermodynamics-based approach. Microscopy, X-ray diffraction analysis, infrared

20 spectroscopy, nuclear magnetic resonance, and thermogravimetric analysis provided complimentary

21 characterisation. Mechanochemical synthesis of LID:AZE systems at a range of stoichiometries yielded

22 at least two distinct liquid phases and two distinct crystalline phases, one of which involved a unique

23 2:3 LID:counterion composition not observed previously. Furthermore, to the best of our knowledge

24 the formation of oligomeric ionic liquids involving dicarboxylic acids is also being reported for the first

25 time. This work highlights the need for a careful characterisation of multicomponent systems,

26 especially for pharmaceutical applications.

27

28

30

1. Introduction

A number of interesting works have been published very recently raising awareness on the continuum that exists between ionised and neutral pharmaceutical multicomponent systems.[1–3] A change in preparation methods, temperature or stoichiometry can modulate the ionic character of the system and yield different products as a result of complex interrelationship of kinetic and thermodynamic aspects.[1,4–6] In particular, there are examples illustrating that distinct crystalline structures obtained by varying stoichiometry of co-formers or counterions can tune the solid state properties and performance of an active pharmaceutical ingredient (API).[7–9]

Although, the majority of the investigated pharmaceutically-relevant API multicomponent systems are crystalline the rising significance of low-melting point solids or even liquid forms of such systems has been recognised.[10–15] They include, but are not limited to ionic liquids, deep eutectic mixtures, ionic cocrystals and oligomeric ionic liquids. Until recently, the intermolecular interactions that play the major role in the classification of the liquid forms were mainly considered at simple 1:1 stoichiometric ratios and stoichiometries dictated by the counterion of choice.[16,17] On the other hand, non-stoichiometric ratios were viewed as systems containing excess of either of the starting materials.[18] However, it has been shown that mixtures of the counterions or the co-formers at different stoichiometric ratios can potentially form distinct multicomponent systems not just in the solid but also in the liquid state.[2,19]

Our previous work concentrated on a range of API-ILs incorporating lidocaine and medium-chain dicarboxylic acids as the counterions. [20] LID is an aminoamide drug used as a local anaesthetic with some antibacterial properties [21] and the molecule possesses one H-bond donor -NH group and 3 H-bond acceptor groups (**Scheme 1**). LID is practically insoluble in water and is formulated as a salt to overcome the solubility constraints. The tertiary amine group has a pKa value of 7.9 rendering it a weak base and most of the known LID salts undergo ionisation at this site.[22,23] However, in an ionised form LID's membrane permeability is severely impeded.[24] Careful co-former or counterion selection for a new LID multicomponent phase formation can greatly improve the API's performance

3

58   without undergoing chemical modification.[14,25,26] The LID ionic liquids (ILs) based on medium-

59   chain dicarboxylic acids were evaluated in terms of their thermal and dynamic behaviour supported

60   by crystallographic analysis in an attempt to devise a prediction tool for the structure–property

61   relationship. Alternating trends in morphology, melting points, glass transition temperatures and

62   crystallographic properties of the new phases were observed depending on the acid used. [20]

63   In this work we have investigated the influence of changing stoichiometry of LID and azelaic

64   acid (AZE), another medium-chain dicarboxylic acid on the physicochemical properties of their

65   corresponding multicomponent systems using a thermodynamics-based approach, which includes the

66   construction of the solid-liquid binary phase diagrams. Microscopy, X-ray diffraction analysis, infrared

67   spectroscopy, nuclear magnetic resonance, and thermogravimetric analysis provide complimentary

68   characterisation. The molecular structures of LID and the dicarboxylic acid investigated in the study

69   are shown in **Scheme 1**. AZE is a dicarboxylic acid commonly used as a topical bactericidal, antioxidant

70   and anti-inflammatory agent.[27–29] AZE is a weak acid with 2 carboxylic acid moieties at both ends

71   of the alkyl chain with pKa values of 4.550 and 5.498. The differences in pK$_a$ values (i.e. ΔpK$_a$ = pK$_a$(base)

72   – pK$_a$(acid) are 3.35 and 2.4 meaning that both, salts and cocrystals could potentially be formed.[30]

73   Other known LID:dicarboxylic acid multicomponent systems reported to date were solely ionized

74   systems.[20,23,31] It was thus hypothesised that the LID:AZE combination would yield a similar

75   LID:dicarboxylic acid system. However, mechanochemical synthesis of LID:AZE systems yielded at least

76   two distinct liquid phases and two distinct solid phases, one of which involved a unique 2:3

77   LID:counterion composition not observed previously. Furthermore, to the best of our knowledge the

78   formation of oligomeric ionic liquids involving dicarboxylic acids have been reported for the first time.

79   **2. Materials and Methods**

80   **2.1 Materials**

81   LID (as a base) and azelaic acid (AZE) were purchased from Sigma-Aldrich (Ireland). Potassium

82   bromide for Infrared analysis was obtained from Honeywell Fluka and was dried in a vacuum oven at

83 room temperature prior to use. The purity of the compounds was at least 98%. All compounds were

84 used as obtained. Absolute ethanol used was of HPLC grade (Fisher Scientific, UK).

85 **2.2 Methods**

86 *2.2.1 Sample preparation*

87 LID and AZE was processed at a range of molar fractions between 0.1:0.9 to 0.9:0.1 (LID:AZE).

88 The constituents were accurately weighted with a Mettler Toledo MT5 microbalance (Mettler Toledo,

89 Switzerland) and ground in an agate mortar and pestle until homogenous mixtures were obtained. A

90 total of 200 mg of each sample was produced. A sample of each mixture was immediately analysed

91 and the remaining mixtures were transferred to 2 mL microcentrifuge tubes and kept at 4 °C until

92 further analysis.

93 *2.2.2 Polarised Optical Microscopy*

94 Prior to analysis LID and AZE were recrystallised from ethanol. A small crystal of each, LID and

95 AZE, were placed on a glass slide and were pushed together with the help of a needle. The glass slide

96 was examined using Olympus BX53 polarising optical microscope (Ireland) equipped with a U-POT

97 cross polarizer and a U-ANT analyser. Images were taken with an integrated Q IMAGING Fast 1394

98 camera (Olympus, Japan). The experiment was performed at room temperature.[20]

99 2.2.3 *Thermogravimetric Analysis (TGA)*

100 TGA was performed using Mettler TG50 measuring module coupled to a Mettler Toledo MT5

101 balance (Switzerland). Samples were weighed into an open aluminium pan (sample size approximately

102 5-11 mg) and heated from 25 °C to 200 °C at a rate of 10 K min^{-1} under nitrogen as a purge gas. Upon

103 completion the samples were visually inspected and the thermograms were analysed for degradation

104 using Mettler Toledo STARe software (version 6.10).

105 *2.2.4 Differential Scanning Calorimetry (DSC)*

106   DSC measurements were carried out using a PerkinElmer Pyris1 Diamond DSC unit (USA). The

107   unit was refrigerated using a ULSP B.V. 130 cooling system (Netherlands). [20,32] Approximately 3-6

108   mg samples were weighed into aluminium pans and sealed. The samples were heated from 25 °C to

109   115 °C at the rate of 10 K min^{-1} with nitrogen at a flow rate of 40 mL min^{-1} used as the purge gas. The

110   samples were then supercooled to -60 °C at 300 K min^{-1} cooling rate and a second heating cycle was

111   performed. Thermograms were analysed using Perkin Elmer Pyris software.

112   *2.2.5 Fourier-Transform Infrared (FTIR) analysis*

113   Prior to analysis LID:AZE mixtures at selected compositions were heated at 60 °C under

114   nitrogen gas for 30 min to remove moisture. The samples were prepared as KBr disks using direct

115   compression using a hydraulic press. Sample loading was approximately 1% (w/w). Infrared spectra

116   were recorded on Spectrum One spectrometer (Perkin Elmer, USA). A spectral range of 650-4000 cm^{-1}

117   and accumulation of 8 scans were used. Spectra was analysed using Spectrum v. 5.0.1 software.

118   *2.2.6 Powder X-ray Diffraction (PXRD) analysis*

119   The LID:AZE samples were prepared at room temperature and were kept at 4 °C prior to

120   analysis. PXRD was carried out at room temperature using Rigaku Miniflex II X-ray diffractometer

121   (Japan) equipped with Cu Kα radiation (1.54 Å) X-ray source. The samples were scanned over a 2θ

122   degrees range of 2–40° with a scan rate of 0.05 °/s. The tube voltage and tube current used were 30 kV

123   and 15 mA, respectively. [20]

124   *2.2.7 Single Crystal X-ray Diffraction (SXRD)*

125   Preparation of Phase 1 (2:1 LID:AZE cocrystal) - A sample of LID:AZE at equimolar composition

126   was heated until freely flowing liquid was obtained. The liquid sample was poured inside an NMR tube

127   and was kept in the fridge until crystals were observed.

128   Preparation of Phase 2 (2:3 LID:AZE ionic liquid) - Solidified polycrystalline powder at 1:1 molar

129   composition was obtained upon prolonged storage for 6 months at room temperature. A few crystals

130   were removed with a needle to be seeded onto a drop of liquefied 1:2 LID:AZE mixture on a glass slide

131   and kept at room temperature. Larger crystals of satisfactory quality for SXRD analysis were harvested

132   after a week.

133   Data for 2:1 LID:AZE cocrystal and 2:3 LID:AZE salt samples were collected on a Bruker Apex

134   Kappa Duo using Cu Kα radiation (λ = 1.54178 Å) using a MiTeGen microloop and at 100(2) K (Oxford

135   Cobra Cryosystem). Bruker APEX [33] software was used to collect, correct (Lorentz and polarization)

136   and reduce data. Absorption corrections were applied using SADABS.[34] The structure was solved

137   with the SHELXT [35] structure solution program using Intrinsic Phasing and refined with the SHELXL

138   [36] refinement package using Least Squares minimisation with Olex2[37], using the space group $P2_1$,

139   with Z = 2 for the formula unit, $C_{37}H_{60}N_4O_6$. Details of the data and refinement are given in **Table S1**.

140   All non-hydrogen atoms were refined anisotropically. Hydrogen atoms were assigned to calculated

141   positions using a riding model with appropriately fixed isotropic thermal parameters; donor hydrogen

142   atoms (H9a, H9b, 18, H30) were located and refined with restraints (DFIX). The absolute configuration

143   was determined and confirmed by refining the Flack parameter as 0.3(2). CCDC 2098381 (Phase 1) and

144   2098382 (Phase 2) contain the supplementary crystallographic data for this paper. The data can be

145   obtained   free   of   charge   from   The   Cambridge   Crystallographic   Data   Centre   via

146   www.ccdc.cam.ac.uk/structures. The pXRD and SXRD were compared using EXPO2014 [38] with a final

147   Le Bail refinement using the Pearson VII peak shape function with a w= 1.0/count weighting scheme.

148   Final agreement factors, 2:1 LID:AZE cocrystal : Rp = 10.017, Rwp = 14.605, Re = 4.926 and Chi2 =

149   8.791; 2:3 LID:AZE salt : Rp = 7.525, Rwp = 10.284, Re = 6.203, Chi2= 2.748.

2.2.8 Proton Nuclear Magnetic Resonance (^{1}H-NMR)

151   Crystalline 1:1 LID:AZE sample obtained upon prolonged storage at room temperature and 2:1

152   LID:AZE sample freshly prepared by neat grinding were dissolved in DMSO-d_6. ^{1}H-NMR measurements

153   were performed using Bruker Avance III 400 MHz spectrometer. The NMR spectra were analysed using

154   TopSpin 4.0.9 software. See **SI and Figure S1** for the ^{1}H-NMR peak assignment.

3. Results and discussion

3.1 Morphology of samples

The study was initiated by solvent-free neat grinding mechanochemical synthesis of the LID:AZE systems at 0.1:0.9 – 0.9:0.1 molar compositions. Samples in the χ_{LID} = 0.33 to 0.66 range yielded semiliquid or soft solid (paste) samples at room temperature (**Figure 1a**). On the contrary, systems at extreme molar LID or AZE molar fractions were solid powders. POM analysis was performed to visually examine the process of liquefaction. The POM images in **Figure 1b** display the solid fusion experiment where recrystallised LID and AZE were placed side by side and solid state reactivity was observed. Crystalline regions that were in a direct contact started undergoing liquefaction at room temperature almost immediately and a noticeable change was observed at *t* = 10 min. At *t* = 7 days the entire interface has liquefied. This observation indicates that the melting point of the product of the solid-state reaction is below room temperature and such behaviour is characteristic of a liquid, or a "deep", eutectic formation.[20,39,40] The remaining crystalline material that was not in a direct contact has not been altered signifying the liquid eutectic does not diffuse nor dissolve parent materials further. POM image in **Figure 1c** obtained at *t* = 14 days displays the formation of new dendritic structures. These structures may suggest an irregular eutectic morphology of this phase and/or a new phase formation.[41] Previously, POM demonstrated that LID reacted with glutaric acid or pimelic acid showed a similar behaviour and these LID:dicarboxylic acid mixtures underwent solid interdiffusion, while LID and suberic acid displayed true solid-state reactivity with the formation of a solid eutectic at the interface. [20]

3.2 Thermal analysis

Starting materials LID and AZE as well as their mixtures at three different molar compositions (2:1, 1:1 and 2~~1~~:2~~1~~ LID:AZE) were analysed for thermal degradation by TGA (**Figure 2a**). The results showed that the weight loss upon heating up to 120 °C did not exceed 2%, see **Figure 2b and c**~~b~~. Heating of the materials up to 120 °C generally results in dehydration or solvent evaporation. A very

8

180 slight increase in weight loss exhibited by the binary mixtures might be associated with increased

181 hygroscopicity of the samples following mixing. This observation is not unusual as it has been shown

182 that low melting systems generally display elevated hygroscopicity.[13] On the other hand, upon

183 heating to 200 °C the % weight loss is mainly caused by sample degradation. In this case LID and 2:1

184 LID:AZE underwent extensive degradation. However, upon addition of increased amount of AZE the

185 degradation was decreased. These results are also illustrated by the sample colour change after the

186 analysis. As seen in **Figure 2a** 2:1 LID:AZE mixture turned very dark brown as compared to lighter

187 brown colours of 1:1 and 1:2 samples.

188   DSC analysis of freshly prepared samples was carried out to study the phase change behaviour

189 of the LID:AZE systems at various molar compositions. **Figure 3a** presents a stack of DSC thermograms

190 of the first heating cycle at different LID:AZE molar compositions. LID and AZE exhibit sharp

191 endothermic peaks corresponding to their melting points of 69 °C and 106 °C, respectively. The

192 melting point depression of LID is observed and is indicated by a blue arrow as increasing molar

193 concentrations of AZE are added to the binary mixtures. A similar melting point depression is observed

194 in AZE (indicated by a brown arrow) with increasing LID content. This observation follows simple binary

195 phase behaviour as a result of decreasing purity of the starting components and has been observed in

196 numerous multicomponent systems previously.[42,43] In addition to the endothermic peaks

197 corresponding to the fusion events of the starting components the presence of new endothermic

198 peaks in LID:AZE mixtures indicates the formation of new crystalline arrangements. As visible from the

199 endothermic peaks in the yellow box the mechanochemical grinding of LID and AZE at high LID molar

200 concentrations leads to a new phase formation, referred to as Phase 1. At χ_{LID} = 0.6 and 0.55 a melting

201 point depression of this Phase 1 is observed. The evolution of a double peak unique to 1:1 molar

202 composition infers the coexistence of two distinct crystalline arrangements. However, the second

203 peak is not easily discerned in samples with higher AZE content, probably due to the creation of

204 additional hydrogen bonds between the new crystalline structure and free diacid which leads to

205 further sample liquefication. This phenomenon has been described previously in the formation of

9

206   deep eutectic mixtures (DEMs) and oligomeric ionic liquids.[44,45] It has been shown, but not

207   generally recognised, that other forms of ionic liquids and DEMs can form at non-stoichiometric

208   compositions and it is not just a 1:1 ionic liquid with excess carboxylic acid.[19,46–48] It has been

209   proposed that such arrangement in the liquid phase can be described as $[BH^+][(RCOO)_2H^-]$.[18] The

210   inherent slow crystallisation kinetics of these systems hinders phase identification. In an attempt to

211   curtail liquefaction samples in the range of χ_{LID} = 0.9 to 0.2 were prepared and stored in the fridge for

212   1 day prior to analysis. As indicated by a red box and arrow in **Figure 3b**, this sample treatment method

213   enhanced new phase crystallisation, referred to as Phase 2.

214   Experimental T_m values were plotted as a function of LID molar fraction as seen in **Figure 4**.

215   Dashed lines represent theoretical Schroeder van Laar solubility curves calculated using **Equation 1**,

216   where T_{fus} (K) denotes the temperature of fusion and ΔH_{fus} (J mol^{-1}) denotes the enthalpy of fusion of

217   the pure starting component, χ is the mole fraction of the pure starting component at a specified

218   temperature T (K), and R is the gas constant.

219    $$T = \left(\frac{1}{T_{fus}} - \frac{R \ln \chi}{\Delta H_{fus}} \right)$$ **(Eq. 1)**

220   It is evident that the melting points of the parent components can be reasonably predicted at their

221   corresponding extreme molar fractions. This agreement suggests that the unreacted starting

222   components remain in the mixture in their unchanged form and no additional intermolecular

223   interactions are depressing their corresponding T_m. However, the T_m of the parent components

224   disappear at 0.3:0.7 – 0.6:0.4 LID:AZE molar compositions. This region is highlighted in **Figure 4**. This

225   observation suggests new intermolecular interactions being created within the system and is

226   corroborated by the appearance of melting events of Phase 1 and Phase 2. It is interesting to note that

227   at the equimolar composition the melting events of the these phases merge, thus creating a sensitive

228   equilibrium where the identity of phase formation depends on fine sample preparation and storage

229   variables.

230   Upon completion of the first heating step the samples at the entire range of compositions

231   were fast cooled at a nominal rate of 300 K/min and then subjected to a second heating step. **Figure**

232   **S2** presents a stack of second heating DSC thermograms which reveal the presence of glass transition

233   events (T_g) in LID:AZE mixtures which implies the ability of the systems to be supercooled. Pure starting

234   components do not exhibit T_g transitions as they crystallise during the cooling step. It is important to

235   note that the samples at the extreme LID and AZE compositions also undergo partial crystallisation

236   upon cooling and the T_g values of these systems are indicated by open star symbols in **Figure 4**. As can

237   be seen from **Figure 4**, there is a clear maximum in T_g at the equimolar composition of the acid and

238   the base. The observed extremum in T_g behaviour can be explained in terms of ionicity degree.

239   Previously, a marked increase in T_g has been correlated with the conversion of a given API into its

240   corresponding salt form e.g. hydrochloride, sulphate or phosphate.[44,49] Moreover, it has been

241   established that an increase in the T_g and melting point of classical aprotic ionic liquids is observed

242   when the electrostatic interactions start to dominate van der Waals forces.[50] Consequently, it is

243   expected that the supercooled equimolar LID:AZE system exhibits the most efficient proton transfer

244   and thus, comprises the highest concentration of ionised species.

245   *3.3 Investigation of ionicity in the supercooled state*

246   FTIR spectroscopy was employed to investigate the changes in intermolecular interactions

247   within the liquid systems as a function of LID:AZE molar composition (**Figure 5a**) to corroborate the

248   results obtained by thermal analysis. The systems were melted and analysed by FTIR immediately to

249   mimic the supercooled state investigated by the second DSC heating cycle. The clear T_g maximum

250   observed at the equimolar LID:AZE composition suggests the highest degree of ionisation and thus,

251   ionic liquid formation. One of the most prominent peaks observed corresponds to the carbonyl

252   stretching vibration and appears at 1664 cm^{-1} and 1694 cm^{-1} in LID and AZE spectra, respectively. The

253   magnified carbonyl region is presented as an inset in **Figure 5b** for clearer visualisation. However,

254   spectra obtained for the binary LID:AZE mixtures exhibit an additional carbonyl signal not attributable

255   to parent materials. This phenomenon is most clearly visible in the mixtures with higher LID content.

256   In the 2:1 LID:AZE supercooled sample the signal is found at 1717 cm^{-1} and its position is shifted to

257   1724 cm^{-1} in 1:1 supercooled LID:AZE mixture. In χ_{LID} = 0.4 mixture the peak appears as a shoulder at

258   around 1717 cm^{-1}. The emergence of this peak may imply the formation of intermolecular H-bonds

259   between the -NH moiety of the LID's amide group and the carbonyl group of the AZE. As a result of -

260   NH group participating in the creation the new H-bond, the C=O bond is strengthened and a shift to

261   higher wavenumbers is observed. The greatest shift at the 1:1 composition suggests the strongest

262   amide-carbonyl H-bond formation, most probably due to formation of the homogenous 1:1 molecular

263   arrangement. This reasoning is corroborated by the complete disappearance of pure LID signal as a

264   result of being entirely used up in the 1:1 complex formation. Hence, giving rise to the observed T_g

265   maximum. On the other hand, AZE C=O signal persists in the spectrum, which can be explained by the

266   availability of 2 carbonyl groups and 1 being left unchanged. In addition, a prominent symmetric

267   stretching carboxylate ion peak at 1540 cm^{-1} appears in the spectra of mixtures, which provides an

268   indication that ionisation in the form of proton transfer between LID and AZE has taken place.

269   The decreased intensity and wavenumber of the amide N-H stretch at 3250 - 3170 cm^{-1} region

270   is caused by the dilution of LID in AZE and the formation of the H-bond (*vide supra*). A peak assignment

271   table is presented in **Table S2**. The presence of proton transfer in the 1:1 complex implies the

272   formation of an ionic liquid. The systems with the higher acid content, i.e. in the range χ_{LID} = 0.4 to

273   0.33 possess a greater number of hydrogen bonds formed within the complexes and, as a result, the

274   systems are further liquefied. Depending on the arrangement of these additional H-bonds formed the

275   compositions may be classified as either oligomeric ionic liquids or deep eutectic mixtures.

276   *3.4 Investigation of crystalline phases*

277   PXRD analysis of the samples prepared as described in Section 2.2.1 revealed the formation

278   of a new crystalline phase at χ_{LID} = 0.5 to 0.2 range of compositions, as seen in **Figure 6**. Melting of this

279   this new system, Phase 2, was first observed by thermal analysis (Figure 4). The PXRD pattern

280   corresponding to the new phase displays peaks that do not appear in the patterns on the parent

281   materials, such as at $2\theta = 6°$, $11°$, $14°$ and $16°$. Low intensities of the peaks were observed due to the

282   sample being partially liquid. A peak at $2\theta = 6°$ appears at a lower position as compared to the first

283   peaks of the parent materials signifying the formation of a larger crystal lattice.

284   An attempt to obtain a single crystal of Phase 2 has unexpectedly resulted in an identification

285   of a second, new crystalline phase, Phase 1. The PXRD pattern of this system is highlighted in red

286   colour in **Figure 6** and appears to be very similar to pure LID with some differences. In particular, the

287   2:1 system displays a peak at $2\theta = 8.4°$ as compared to a peak at $2\theta = 8.2°$ seen in LID, and displays

288   unique peaks at $2\theta = 11°$, $18°$, $24°$, $27°$ and $28°$. These peaks are also visible in the pattern of the χ_{LID}

289   = 0.5 mixture implying sample heterogeneity, where both new crystalline products coexist in

290   equilibrium.

291   *3.5 Effects of sample preparation and storage on systems speciation*

292   It is important to note the impact of method of sample preparation and storage conditions on

293   the LID:AZE complex formation. DSC analysis was performed using freshly ground samples without

294   preheating in order to capture any thermal transitions that occur at lower temperatures. For example,

295   a freshly ground 1:1 LID:AZE sample appears as a liquid (**Figure 1a**) with a small amount of solid

296   particles suspended within the liquid matrix. These particles were later identified as nucleation sites

297   for the formation of the new crystalline complexes (Phase 2) and DSC thermograms of these samples

298   allowed to capture their melting points. However, preheating 1:1 LID:AZE samples up to 60 °C in an

299   oven destroyed these crystallisation nucleation sites resulting in a stable for at least 6 months ionic

300   liquid that did not crystallise on storage at room temperature. PXRD analysis of the freshly ground

301   samples allowed identification of the new crystalline structures being formed from these nucleation

302   sites, these crystals showed distinct PXRD patterns as seen in **Figure 6**. PXRD analysis of the equimolar

303   sample performed after preheating did not display any diffraction peaks and resulted in a disordered

304   "halo". The samples with the higher AZE content exhibited analogous behaviour. Therefore, it is

13

305 possible to conclude that LID:AZE molten mixtures form distinct ionic liquid phases at a range of

306 equimolar and non-stoichiometric ratios with greater acid content.

307　　　On the other hand, the base-rich 2:1 LID:AZE mixture was not as sensitive to environmental

308 variables. Crystalline Phase 2 was successfully obtained by both methods, neat grinding at room

309 temperature and co-melting parent components in an oven. Another important observation to note

310 is the equilibrium of the 2:1 and 1:1 complex formation in the LID:AZE equimolar mixtures. Depending

311 on the preparation and storage conditions different crystalline phases were observed and the

312 summary of the observations in presented in **Table 1**. The bulk synthesis of Phase 2 not successful.

313 A range of seeding experiments were also attempted, where a polycrystalline impure Phase 2 was

314 seeded in a molten equimolar LID:AZE mixture, in a molten 1:2 LID:AZE mixture and in multiple organic

315 solvents. The impure Phase 2 contained a mixture of crystalline LID and both of the crystalline systems.

316 As a result, in most cases an identical impure polycrystalline material was obtained. These results can

317 be explained by the differences in the stability and solubility exhibited by these complexes, where the

318 least soluble and most stable system crystallising out first. This phenomenon has been identified and

319 investigated in other binary systems with LID [51] and other APIs [1,52,53]. However, seeding in a

320 molten acid-rich 1:2 mixture yielded a pure Phase 1 crystal with quality satisfactory for SXRD analysis.

321 The crystallisation work performed with LID:AZE mixtures was very challenging and before single

322 crystals were obtained a suspicion was raised that one of the crystalline phases might actually be a

323 degradation product. To check for sample degradation ^{1}H-NMR analysis was performed. The peak

324 assignment presented in **Figure S1** indicates that Phase 1 and Phase 2 differ in the solid state, but

325 degradation products were not observed in the ^{1}H-NMR spectra.

326 *3.6 Single Crystal XRD analysis*

327　　　Single crystals of the two distinct crystalline phases, Phase 1 and Phase 2, were obtained and

328 analysed. Phase 1, the 2:1 LID:AZE complex with a melting point of 47 °C and crystallising in a

329 monoclinic P2$_1$ space group was identified as a cocrystal. The theoretical PXRD pattern generated from

330 the SXRD data closely matched experimental PXRD patterns by visual inspection and a Le Bail

14

331 refinement with difference pattern shown in **Figure S3**. The asymmetric unit contains 2 LID molecules

332 and 1 AZE molecule held together by H-bonding interactions as seen in **Figure 7a**. The strongest H-

333 bonds are formed between the LID tertiary amine moiety and both AZE carboxylic groups with d(D...A)

334 = 2.583(3) and 2.603(3) Å. The formation of a cocrystal, rather than a salt is also evidenced by the AZE

335 carboxylic C-O bond length analysis. In salts, the deprotonation of a carboxylic acid results in a

336 carboxylate ion possessing two C-O bonds with similar D_{C-O}, i.e. the $\Delta D_{C-O} < 0.03$ Å, where ΔD_{C-O} is the

337 difference in length between the two C-O bonds within a carboxylate moiety. In cocrystals, neutral

338 carboxylic acids would possess two distinct C-O bonds with $\Delta D_{C-O} > 0.08$ Å.[54] The 2:1 LID:AZE complex

339 exhibits high ΔD_{C-O} values of 0.119 and 0.125 Å confirming cocrystal formation. The crystal structure is

340 further stabilised by the hydrogen-bonded NH...O heterosynthons (d(D...A) = 2.900(3) and 2.932(3) Å)

341 formed between the LID amide moieties and further weak CH...O interactions (d(D...A) = 3.243(3) Å).

342 The resulting structure forms zig-zag crystallisation patterns as seen in **Figure 7b**. See **Figure S5** and

343 **Table S3** for atom labels and a list of all hydrogen bonds present within the system.

344   Interestingly, despite the fact that the crystalline 2:1 LID:AZE system is a cocrystal, FTIR

345 analysis showed that the carboxylate ion peak was also visible in the supercooled mixture of the same

346 composition (**Figure 5**). This is due to the ability of the system to be partially liquified as indicated by

347 the presence of a Tg transition observed by DSC (**Figure 4**). Hence, the supercooled fraction of the

348 sample exhibits proton transfer due to increased molecular mobility.

349   The second crystalline phase, Phase 2, comprises a highly unusual 2:3 LID:AZE ratio and it is

350 characterised by a melting point onset of 50 °C. No other crystalline structures involving LID at such

351 ratio with other counterions or co-formers has been deposited in the CSD database to date. The

352 complex crystallises in a triclinic P$\bar{1}$ space group with 2 LID and 3 AZE molecules constituting an

353 asymmetric unit. Theoretical PXRD patterns generated from the SXRD data closely match

354 experimental PXRD patterns by visual inspection and a Le Bail refinement with difference pattern

355 shown in **Figure S4**. The crystalline structure is composed of 2 unionised AZE molecules, 1 doubly

356 ionised AZE anion and 2 ionised LID cations which are held together via a complex network of

357 hydrogen bonding interactions as seen in **Figure 8a-b**. The 2 LID molecules are ionised at the tertiary

358 amine sites via a proton transfer from both carboxyl moieties of a single AZE molecule. The complete

359 deprotonation of AZE is supported by C-O bond analysis, where the two carboxyl moieties possess

360 ΔD_{C-O} of 0.004 and 0.006 Å. The deprotonated carboxylate anions form hydrogen bonding interactions

361 with $LIDH^+$ cations via all possible amine and amide H-bond donors, the strongest of which occurs

362 between the carboxylate anion and an amide moiety COO-…NH with d(D…A)= 2.811(6) Å. The doubly

363 deprotonated AZE anion is further stabilised by H-bonds arising from unionised AZE carboxyl donors

364 with d(D…A) distances ranging from 2.559(6) to 2.633(6) Å. See **Figure S6** and **Table S4** for atom labels

365 and a list of all hydrogen bonds present within the system. The structure is highly complex which

366 explains the great difficulty faced during crystallisation efforts.

367 The molecular arrangement resembles the bonding pattern characteristic of oligomeric ionic

368 liquids. However, all oligomeric ILs reported to date are formed from monocarboxylic acids and the

369 generalised molecular formula is generally accepted as $[BH^+][(RCOO)_2H^-]$.[18] The LID:AZE complex

370 presented in this paper is the first example of oligomeric ionic liquid composed of anions derived from

371 dicarboxylic acids. The molecular formula of the crystalline oligomeric complex may be written as

372 $[(BH^+)_2][(HOOCRCOOH)_2(OOCRCOO)^{2-}]$. Due to the presence of a greater number of H-bonding donors

373 and resultant increased complexity of the potential ion patterns the molecular formula characterising

374 this crystalline complex may or may not be applicable to other dimeric or higher order oligomeric

375 anions and ionic liquids. It is also important to note that the crystalline structure corroborates the

376 interactions in the solid state and these findings support the presence of analogous interactions in the

377 liquid phase. Therefore, the 2:3 crystalline salt is the equivalent solid structure to the 2:3 oligomeric

378 ionic liquid in the liquid phase. In this context, the molecular formula of the 1:2 LID:AZE oligomeric

379 ionic liquid is $[BH^+][(HOOCRCOO)_2H^-]$.

380 **4. Conclusions**

16

381   This work has highlighted the importance of considering a range of stoichiometric ratios for

382   the formation of multicomponent systems incorporating acid-base pairs. Despite a series of equimolar

383   LID:dicarboxylic acid salts published previously we have demonstrated that LID and AZE binary

384   mixtures at various molar compositions can form a range of distinct multicomponent phases. This

385   approach allows for fine-tuning of physicochemical and crystallisation properties of a binary system

386   without altering its constituents. Neat grinding of LID and AZE has resulted in the formation of liquid

387   or semiliquid systems at the χ_{LID} = 0.33 to 0.66 molar fractions, where 1:1 composition exhibited the

388   highest ionicity attributable to an ionic liquid formation. The greatest extent of liquefaction at χ_{LID} =

389   0.4 was attributed to an oligomeric ionic formation, the crystal structure of which was solved to be a

390   2:3 oligomeric crystalline ionic liquid. To the best of our knowledge, such system is the first example

391   of an oligomeric ionic liquid composed of anions derived from dicarboxylic acids with a

392    $[(BH^+)_2][(HOOCRCOOH)_2(OOCRCOO)^{2-}]$ general molecular formula. In addition, a crystal structure of

393   2:1 LID:AZE cocrystal was also successfully obtained. These results suggest that prediction of acid-base

394   multicomponent systems formation is more challenging when variable stoichiometric ratios are

395   considered. However, addressing the non-stoichiometric approach allows for a better understanding,

396   modification and visualisation of alternative forms of multicomponent phases.

397   **Acknowledgements**

401   **References**

402   [1]   D. Bernasconi, S. Bordignon, F. Rossi, E. Priola, C. Nervi, R. Gobetto, D. Voinovich, D. Hasa,

403   N.T. Duong, Y. Nishiyama, M.R. Chierotti, Selective Synthesis of a Salt and a Cocrystal of the

404   Ethionamide-Salicylic Acid System, Cryst. Growth Des. 20 (2020) 906–915.

405   doi:10.1021/acs.cgd.9b01299.

406   [2]   M.E. Easton, K. Li, H.M. Titi, S.P. Kelley, R.D. Rogers, Controlling the Interface between Salts,

407   Solvates, Co-crystals, and Ionic Liquids with Non-stoichiometric Protic Azolium Azolates,

408   Cryst. Growth Des. 20 (2020) 2608–2616. doi:10.1021/acs.cgd.9b01733.

409   [3]   H. Lengauer, D. Makuc, D. Šterk, F. Perdih, A. Pichler, T.T. Lušin, J. Plavec, Z. Časar, Co-

410   crystals, salts or mixtures of both? The case of tenofovir alafenamide fumarates,

411   Pharmaceutics. 12 (2020) 342. doi:10.3390/pharmaceutics12040342.

412   [4]   D. Wiechert, D. Mootz, Molecular beside ionic: Crystal structures of a 1/1 and a 1/4 adduct of

413   pyridine and formic acid, Angew. Chemie - Int. Ed. 38 (1999) 1974–1976.

414   doi:10.1002/(sici)1521-3773(19990712)38:13/14<1974::aid-anie1974>3.0.co;2-f.

415   [5]   S. Reddy Perumalla, C. Wang, Y. Guo, L. Shi, C.C. Sun, Robust bulk preparation and

416   characterization of sulfamethazine and saccharine salt and cocrystal polymorphs,

417   CrystEngComm. 21 (2019) 2089–2096. doi:10.1039/c8ce01076e.

418   [6]   P. Stainton, T. Grecu, J. Mccabe, T. Munshi, E. Nauha, I.J. Scowen, N. Blagden, First

419   Comparative Study of the Three Polymorphs of Bis(isonicotinamide) Citric Acid Cocrystals and

420   the Concomitant Salt 4-Carbamoylpyridinium Citrate Isonicotinamide, Cryst. Growth Des. 18

421   (2018) 4150–4159. doi:10.1021/acs.cgd.8b00597.

422   [7]   B. Saikia, P. Bora, R. Khatioda, B. Sarma, Hydrogen Bond Synthons in the Interplay of

423   Solubility and Membrane Permeability/Diffusion in Variable Stoichiometry Drug Cocrystals,

424   Cryst. Growth Des. 15 (2015) 5593–5603. doi:10.1021/acs.cgd.5b01293.

425   [8]   Z. Li, A.J. Matzger, Influence of Coformer Stoichiometric Ratio on Pharmaceutical Cocrystal

426   Dissolution: Three Cocrystals of Carbamazepine/4-Aminobenzoic Acid, Mol. Pharm. 13 (2016)

427   990–995. doi:10.1021/acs.molpharmaceut.5b00843.

428   [9]   M. Samipillai, S. Rohani, The role of higher coformer stoichiometry ratio in pharmaceutical

429   cocrystals for improving their solid-state properties: The cocrystals of progesterone and 4-

430   hydroxybenzoic acid, J. Cryst. Growth. 507 (2019) 270–282.

431   doi:10.1016/j.jcrysgro.2018.10.050.

432   [10] C. Agatemor, K.N. Ibsen, E.E.L. Tanner, S. Mitragotri, Ionic liquids for addressing unmet needs

433   in healthcare, Bioeng. Transl. Med. 3 (2018) 7–25. doi:10.1002/btm2.10083.

434   [11] R. Ferraz, L.C. Branco, C. Prudêncio, J.P. Noronha, Ž. Petrovski, Ionic liquids as active

435   pharmaceutical ingredients, ChemMedChem. 6 (2011) 975–985.

436   doi:10.1002/cmdc.201100082.

437   [12] J.L. Shamshina, P.S. Barber, R.D. Rogers, Ionic liquids in drug delivery, Expert Opin. Drug Deliv.

438   10 (2013) 1367–1381. doi:10.1517/17425247.2013.808185.

439   [13] A. Balk, U. Holzgrabe, L. Meinel, Pro et contra' ionic liquid drugs - Challenges and

440   opportunities for pharmaceutical translation, Eur. J. Pharm. Biopharm. 94 (2015) 291–304.

441   doi:10.1016/j.ejpb.2015.05.027.

442   [14] W.L. Hough, M. Smiglak, H. Rodríguez, R.P. Swatloski, S.K. Spear, D.T. Daly, J. Pernak, J.E.

443   Grisel, R.D. Carliss, M.D. Soutullo, J.H. Davis, Jr., R.D. Rogers, The third evolution of ionic

444   liquids: active pharmaceutical ingredients, New J. Chem. 31 (2007) 1429.

445   doi:10.1039/b706677p.

446   [15] A. Umerska, K. Bialek, J. Zotova, M. Skotnicki, L. Tajber, Anticrystal engineering of ketoprofen

447   and ester local anesthetics: Ionic liquids or deep eutectic mixtures?, Pharmaceutics. 12 (2020)

448   368. doi:10.3390/pharmaceutics12040368.

449   [16] B. Nuthakki, T.L. Greaves, I. Krodkiewska, A. Weerawardena, M.I. Burgar, R.J. Mulder, C.J.

450   Drummond, B. Nuthakki, T.L. Greaves, I. Krodkiewska, A. Weerawardena, M.I. Burgar, R.J.

451   Mulder, C.J. Drummond, Protic Ionic Liquids and Ionicity, Aust. J. Chem. 60 (2007) 21–28.

452   doi:10.1071/CH06363.

453   [17] W. Ogihara, H. Kosukegawa, H. Ohno, Proton-conducting ionic liquids based upon multivalent

454   anions and alkylimidazolium cations, Chem. Commun. (2006) 3637–3639.

455   doi:10.1039/B606186A.

456   [18] M.A.R. Martins, P.J. Carvalho, L.M.N.B.F. Santos, S.P. Pinho, J.A.P. Coutinho, The impact of

457   oligomeric anions on the speciation of protic ionic liquids, Fluid Phase Equilib. 531 (2021)

458   112919. doi:10.1016/j.fluid.2020.112919.

459   [19] K.M. Johansson, E.I. Izgorodina, M. Forsyth, D.R. Macfarlane, K.R. Seddon, Protic ionic liquids

460   based on the dimeric and oligomeric anions: [(AcO)xHx-1]-, Phys. Chem. Chem. Phys. 10

461   (2008) 2972–2978. doi:10.1039/b801405a.

462   [20] J. Zotova, Z. Wojnarowska, B. Twamley, M. Paluch, L. Tajber, Green Synthesis of Lidocaine

463   Ionic Liquids and Salts: Mechanisms of Formation and Interactions in the Crystalline and

464   Supercooled States, ACS Sustain. Chem. Eng. 49 (2020) 18266–18276.

465   doi:10.1021/acssuschemeng.0c06811.

466   [21] J. Sedef Gocmen, U. Buyukkocak, O. Caglayan, A. Aksoy, In vitro antibacterial effects of topical

467   local anesthetics, J. Dermatolog. Treat. 19 (2008) 351–353.

468   doi:10.1080/09546630802050498.

469   [22] G.A. Neville, Z.R. Regnier, Hydrogen bonding in lidocaine salts. I. The NH stretching band and

470   its dependence on the associated anion, Can. J. Chem. 47 (1969) 4229–4235.

471   [23] D. Braga, L. Chelazzi, F. Grepioni, E. Dichiarante, M.R. Chierotti, R. Gobetto, Molecular salts of

472   anesthetic lidocaine with dicarboxylic acids: Solid-state properties and a combined structural

473   and spectroscopic study, Cryst. Growth Des. 13 (2013) 2564–2572. doi:10.1021/cg400331h.

474   [24] R. Pérez-Isidoro, F.J. Sierra-Valdez, J.C. Ruiz-Suárez, Anesthetic Diffusion Through Lipid

475   Membranes Depends on the Protonation Rate, Sci. Rep. 4 (2015) 7534.

476   doi:10.1038/srep07534.

477   [25] Y. Miwa, H. Hamamoto, T. Ishida, Lidocaine self-sacrificially improves the skin permeation of

478   the acidic and poorly water-soluble drug etodolac via its transformation into an ionic liquid,

479   Eur. J. Pharm. Biopharm. 102 (2016) 92–100. doi:10.1016/j.ejpb.2016.03.003.

480 [26] P. Berton, K.R. Di Bona, D. Yancey, S.A. A Rizvi, M. Gray, G. Gurau, J.L. Shamshina, J.F. Rasco,

481   R.D. Rogers, Transdermal Bioavailability in Rats of Lidocaine in the Forms of Ionic Liquids,

482   Salts, and Deep Eutectic, ACS Med. Chem. Lett. 8 (2017) 44.

483   doi:10.1021/acsmedchemlett.6b00504.

484 [27] A. Fitton, K.L. Goa, Azelaic Acid: A Review of its Pharmacological Properties and Therapeutic

485   Efficacy in Acne and Hyperpigmentary Skin Disorders, Drugs. 41 (1991) 780–798.

486   doi:10.2165/00003495-199141050-00007.

487 [28] J.P. Leeming, K.T. Holland, R.A. Bojar, The in vitro antimicrobial effect of azelaic acid, Br. J.

488   Dermatol. 115 (1986) 551–556. doi:10.1111/j.1365-2133.1986.tb05764.x.

489 [29] M.A. Sieber, J.K.E. Hegel, Azelaic acid: Properties and mode of action, Skin Pharmacol.

490   Physiol. 27 (2013) 9–17. doi:10.1159/000354888.

491 [30] J. Stoimenovski, E.I. Izgorodina, D.R. MacFarlane, Ionicity and proton transfer in protic ionic

492   liquids, Phys. Chem. Chem. Phys. 12 (2010) 10341–10347. doi:10.1039/c0cp00239a.

493 [31] Z. Wojnarowska, K.J. Paluch, E. Shoifet, C. Schick, L. Tajber, J. Knapik, P. Wlodarczyk, K.

494   Grzybowska, S. Hensel-Bielowka, S.P. Verevkin, M. Paluch, Molecular origin of enhanced

495   proton conductivity in anhydrous ionic systems, J. Am. Chem. Soc. 137 (2015) 1157–1164.

496   doi:10.1021/ja5103458.

497 [32] Z. Wojnarowska, W. Smolka, J. Zotova, J. Knapik-Kowalczuk, A. Sherif, L. Tajber, M. Paluch,

498   The effect of electrostatic interactions on the formation of pharmaceutical eutectics, Phys.

499   Chem. Chem. Phys. 20 (2018) 27361–27367. doi:10.1039/c8cp05905e.

500 [33] Bruker, APEX, (2012).

501   [34]   Bruker, SADABS, (2001).

502   [35]   G.M. Sheldrick, Foundations and Advances SHELXT-Integrated space-group and crystal-

503   structure determination, Acta Cryst. A71 (2015) 3–8. doi:10.1107/S2053273314026370.

504   [36]   G.M. Sheldrick, Crystal structure refinement with SHELXL, Acta Crystallogr. Sect. C Struct.

505   Chem. C71 (2015) 3–8. doi:10.1107/S2053229614024218.

506   [37]   O. V. Dolomanov, L.J. Bourhis, R.J. Gildea, J.A.K. Howard, H. Puschmann, OLEX2: A complete

507   structure solution, refinement and analysis program, J. Appl. Crystallogr. 42 (2009) 339–341.

508   doi:10.1107/S0021889808042726.

509   [38]   A. Altomare, C. Cuocci, C. Giacovazzo, A. Moliterni, R. Rizzi, N. Corriero, A. Falcicchio,

510   EXPO2013: A kit of tools for phasing crystal structures from powder data, J. Appl. Crystallogr.

511   46 (2013) 1231–1235. doi:10.1107/S0021889813013113.

512   [39]   A.P. Abbott, G. Capper, D.L. Davies, R.K. Rasheed, V. Tambyrajah, Novel solvent properties of

513   choline chloride/urea mixtures, Chem. Commun. (2003) 70–71. doi:10.1039/B210714G.

514   [40]   M.A.R. Martins, S.P. Pinho, J.A.P. Coutinho, Insights into the Nature of Eutectic and Deep

515   Eutectic Mixtures, J. Solution Chem. (123AD). doi:10.1007/s10953-018-0793-1.

516   [41]   W. Kurz, D.J. Fisher, Dendrite growth in eutectic alloys: the coupled zone, Int. Met. Rev. 24

517   (1979) 177–204. doi:10.1179/IMTR.1979.24.1.177.

518   [42]   G. Annat, M. Forsyth, D.R. MacFarlane, Ionic liquid mixtures-variations in physical properties

519   and their origins in molecular structure, J. Phys. Chem. B. 116 (2012) 8251–8258.

520   doi:10.1021/jp3012602.

521   [43]   G.J. Maximo, R.J. B N Santos, P. Branda, J.S. S Esperanc, M.C. Costa, A.J. A Meirelles, M.G.

522   Freire, A.P. Coutinho, Generating ionic liquids from ionic solids: An investigation of the

523   melting behavior of binary mixtures of ionic liquids, Cryst. Growth Des. 14 (2014) 4270–4277.

524   doi:10.1021/cg500655s.

525   [44]   J. Stoimenovski, P.M. Dean, E.I. Izgorodina, D.R. MacFarlane, Protic pharmaceutical ionic

526   liquids and solids: Aspects of protonics, Faraday Discuss. 154 (2012) 335.

527   doi:10.1039/c1fd00071c.

528   [45]   K. Bica, J. Shamshina, W.L. Hough, D.R. MacFarlane, R.D. Rogers, Liquid forms of

529   pharmaceutical co-crystals: exploring the boundaries of salt formation, Chem. Commun. 47

530   (2011) 2267–2269. doi:10.1039/C0CC04485G.

531   [46]   S.P. Kelley, A. Narita, J.D. Holbrey, K.D. Green, W.M. Reichert, R.D. Rogers, Understanding the

532   effects of ionicity in salts, solvates, co-crystals, ionic co-crystals, and ionic liquids, rather than

533   nomenclature, is critical to understanding their behavior, Cryst. Growth Des. 13 (2013) 965–

534   975. doi:10.1021/cg4000439.

535   [47]   P. Berton, S.P. Kelley, H. Wang, A.S. Myerson, R.D. Rogers, Separate mechanisms of ion

536   oligomerization tune the physicochemical properties of n-butylammonium acetate: Cation-

537   base clusters vs. Anion-acid dimers, Phys. Chem. Chem. Phys. 19 (2017) 25544–25554.

538   doi:10.1039/c7cp04078d.

539   [48]   K. Bica, R.D. Rogers, Confused ionic liquid ions - A "liquification" and dosage strategy for

540   pharmaceutically active salts, Chem. Commun. 46 (2010) 1215–1217. doi:10.1039/b925147b.

541   [49]   K. Kaminski, E. Kaminska, K. Adrjanowicz, K. Grzybowiska, P. Wlodarczyk, M. Paluch, A.

542   Burian, J. Ziolo, P. Lepek, J. Mazgalski, W. Sawicki, Dielectric relaxation study on tramadol

543   monohydrate and its hydrochloride salt, J. Pharm. Sci. 99 (2010) 94–106.

544   doi:10.1002/jps.21799.

545   [50]   P. Sippel, P. Lunkenheimer, S. Krohns, E. Thoms, A. Loidl, Importance of liquid fragility for

546   energy applications of ionic liquids, Sci. Rep. 5 (2015) 1–8. doi:10.1038/srep13922.

547   [51]   Y. Corvis, P. Négrier, M. Lazerges, S. Massip, J.M. Léger, P. Espeau, Lidocaine/ l -menthol

548   binary system: Cocrystallization versus solid-state immiscibility, J. Phys. Chem. B. 114 (2010)

549   5420–5426. doi:10.1021/jp101303j.

550   [52]   E.A. Losev, E. V. Boldyreva, A salt or a co-crystal-when crystallization protocol matters,

551   CrystEngComm. 20 (2018) 2299–2305. doi:10.1039/c7ce02204b.

552   [53]   Y. Yuan, L. Wang, D. Li, Z. Deng, H. Zhang, How Many Parameters Can Affect the Solid Form of

553   Cocrystallization Products in Mechanochemical Reactions? A Case Study, Cryst. Growth Des.

554   18 (2018) 7244–7247. doi:10.1021/acs.cgd.8b01320.

555   [54]   S.L. Childs, G.P. Stahly, A. Park, The Salt-Cocrystal Continuum: The Influence of Crystal

556   Structure on Ionization State, (2007). doi:10.1021/mp0601345.

557

558

559   Graphical abstract
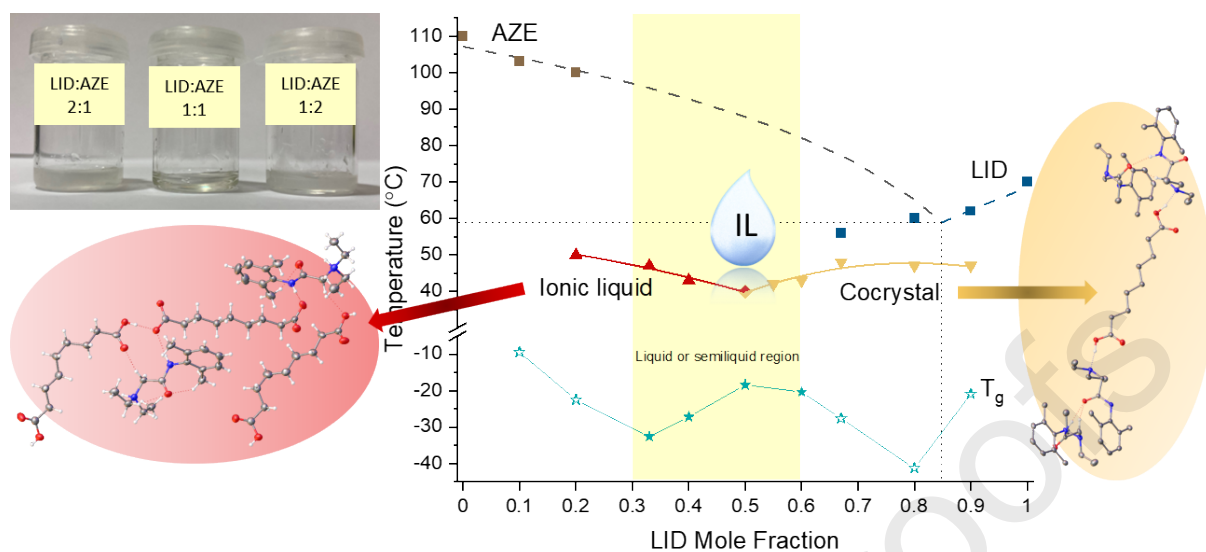
560

561   **Scheme 1**. Molecular structures of LID (left) and AZE (right). Yellow- H-bond donor and acceptor; blue-

562   H-bond acceptor; red- carboxylic acid groups.

563

564   **Table 1**. Impact of preparation and storage variables on phase crystallisation in equimolar LID:AZE

565   mixtures. * Phase 2 was only identified upon prolonged storage (about 3-6 months after sample

566   preparation). ** Only once has this sample crystallised as Phase 2 in an NMR tube and this sample was

567   used for SXRD analysis.

568

569   **Figure 1**. **A**: Photographs of the LID:AZE samples immediately upon grinding. **B**: POM images of the

570   solid fusion experiment. **C**: Interphase at a greater magnification showing dendritic formations.

571   **Figure 2**. **A**: Photographs of the TGA pans after analysis. **B**: TGA degradation profiles of LID, AZE and

572   freshly ground binary mixtures. **C**: Values of % weight loss of LID, AZE and freshly ground binary

573   mixtures upon heating up to 120 and 200 °C.

574 **Figure 3. A** - First heating DSC thermograms of the samples prepared at room temperature; **B** –

575 additional first heating DSC thermograms of the samples prepared at 4 °C. The red dotted line

576 indicates a sample prepared at room temperature and cooled at 4 °C.

577 **Figure 4**. Thermodynamic phase diagram, where T_m of Phase 1 (cocrystal) were obtained from samples

578 prepared at room temperature, while T_m of Phase 2 (ionic liquid) were obtained from samples

579 prepared at 4 °C. Dashed lines represent theoretical Schroeder van Laar solubility lines. Black dotted

580 lines indicate theoretical eutectic composition and T_m. Open star symbols indicate T_g values of the

581 samples that have undergone crystallisation on cooling.

582 **Figure 5**. **A**: FTIR spectra of the LID:AZE systems at various molar compositions. **B**: Inset with magnified

583 carbonyl region of the LID:AZE systems.

584 **Figure 6**. A stack of PXRD traces at the range of LID molar fractions χ_{LID}. The pattern highlighted in red

585 corresponds to Phase 1 and the pattern highlighted in orange corresponds to Phase 2.

586 **Figure 7. A**: Primary hydrogen bonding motif (dotted lines) in the 2:1 LID:AZE cocrystal (Phase 1).

587 Displacement shown at 50% probability. Only hydrogen atoms involved in the H-bonding motif are

588 shown. **B**: Packing diagram of 2:1 LID:AZE viewed normal to the a-axis. Dotted lines indicate hydrogen

589 bonding interactions. Displacement shown at 50% probability.

590 **Figure 8. A**: Primary hydrogen bonding motif (dotted lines) in the 2:3 LID:AZE IL (Phase 2).

591 Displacement shown at 50% probability. Only hydrogen atoms involved in the H-bonding motif are

592 shown. **B**: Packing diagram of 2:3 LID:AZE viewed normal to the a-axis. Dotted lines indicate hydrogen

593 bonding interactions. Displacement shown at 50% probability.

594

595

26

596 **Scheme 1**.

597

598

599

600

601

602
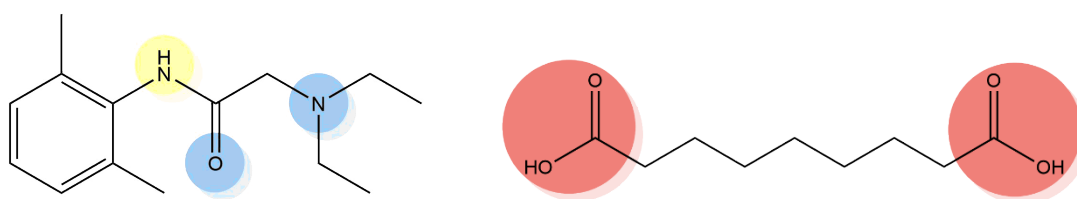
603 **Table 1**.

		Preparation				
		Neat grinding, RT	Neat grinding, 4°C	Co-melting at 60 °C	Seeding in molten 1:1 mixture	Seeding in molten 1:2 mixture
Storage	At RT	Impure polycrystalline	Not performed	Liquid	Impure polycrystalline	**Phase 2**
	At 4 °C	Impure polycrystalline	Impure polycrystalline *	Liquid**	Not performed	Not performed
	Under vacuum	**Phase 1**	Not performed	**Phase 1**	Impure polycrystalline	Not performed

604

605

606

27
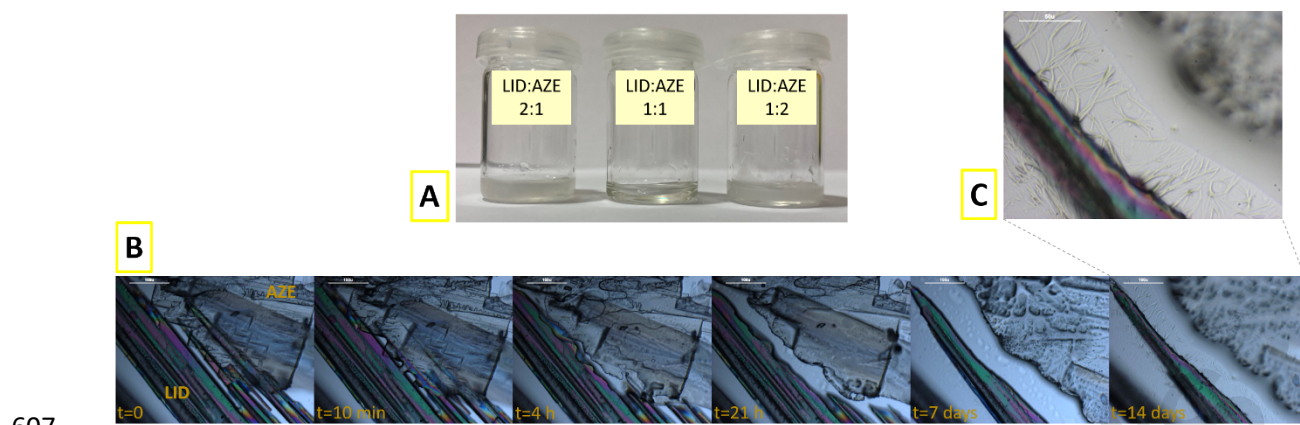
607

608 **Figure 1**.

609

610

611
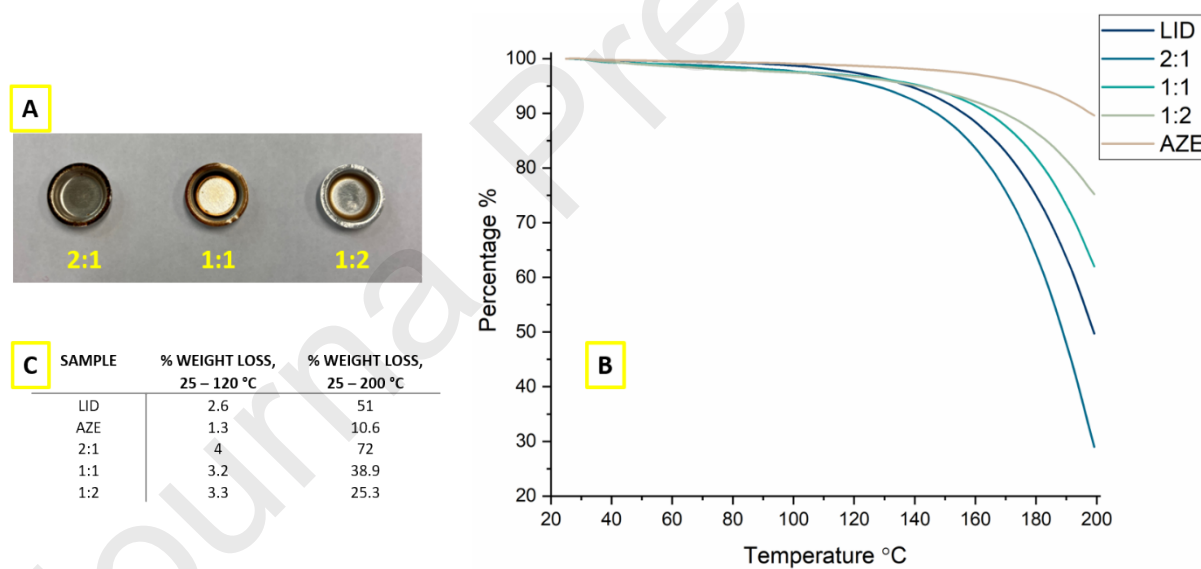
612

613 **Figure 2**.

614

615

Figure 3.

616

617

618
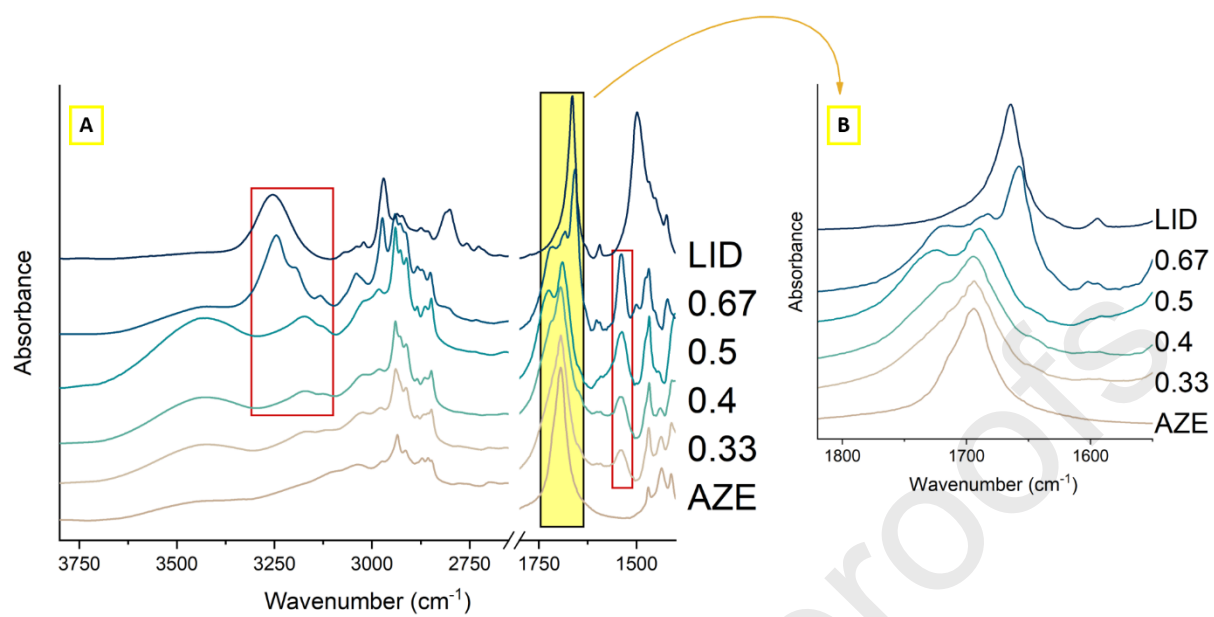

619

Figure 4.

620
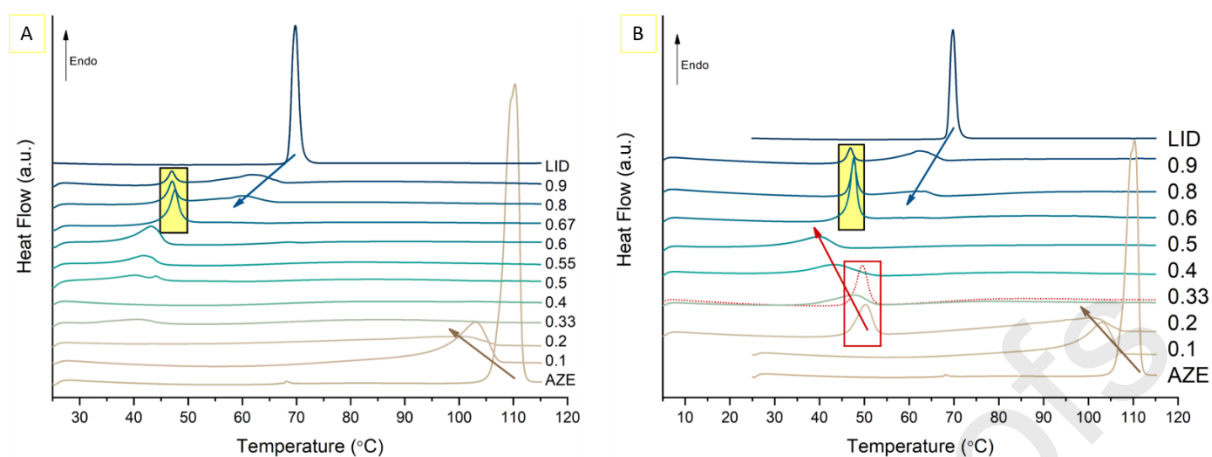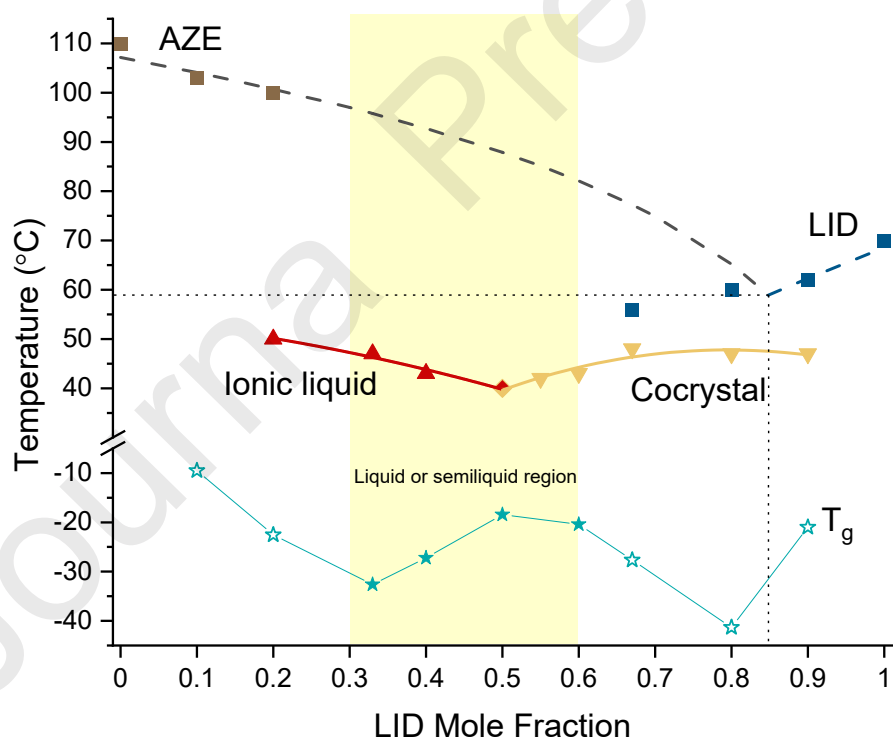
621
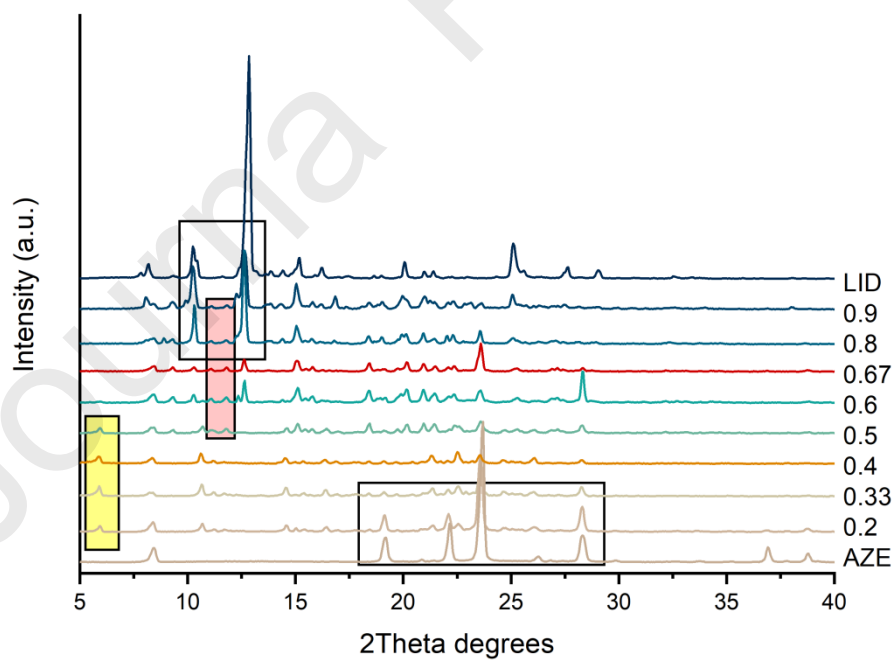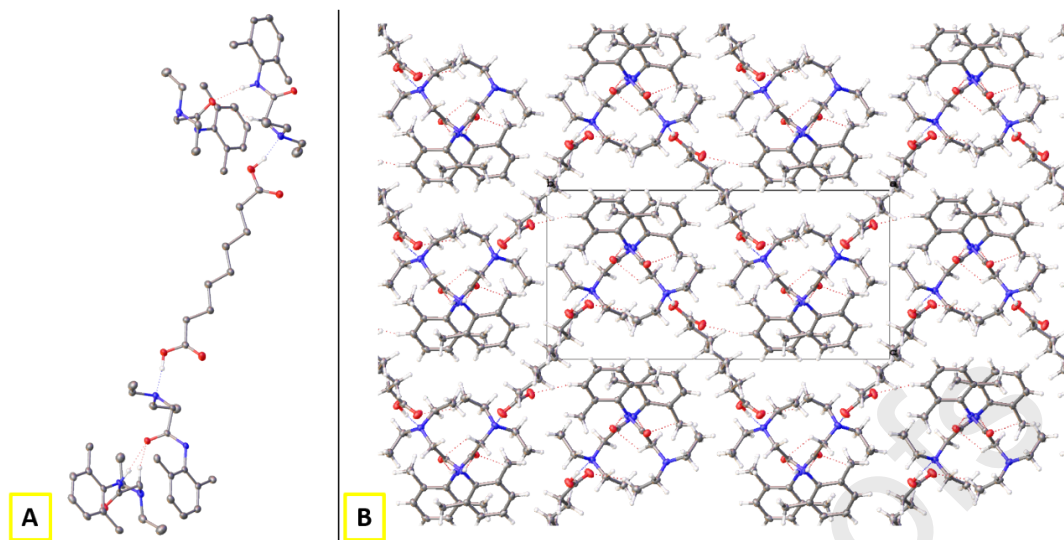
622

623

624 **Figure 5**.

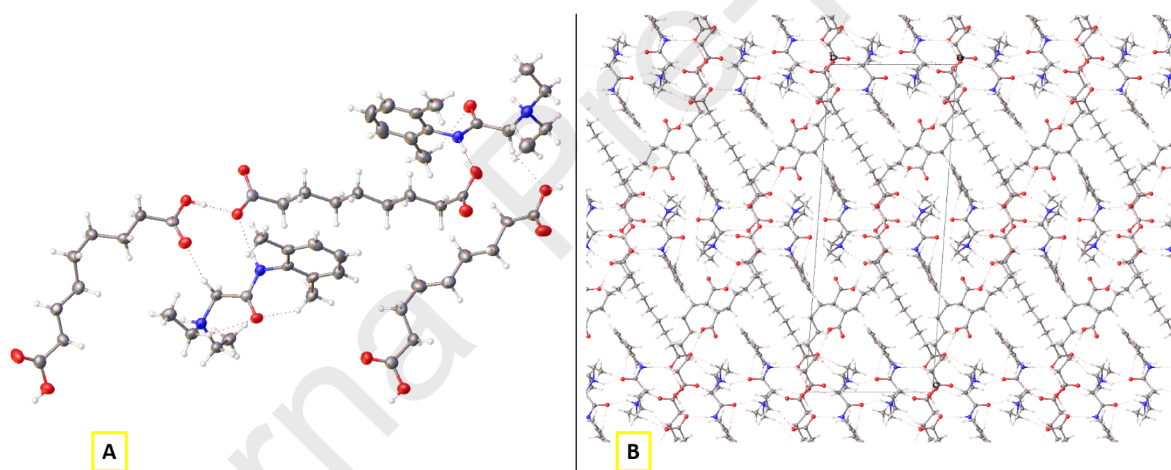625

626

627

628 **Figure 6**.

629

630

631 **Figure 7.**

632

633

634 **Figure 8.**

635

636 **Highlights**

32

637 • First oligomeric ionic liquids made of lidocaine and a dicarboxylic acid was synthesised

638 • The composition of this ionic liquid was 2:3 lidocaine:azelaic acid

639 • A cocrystal phase was also isolated comprising 2:1 lidocaine:azelaic acid

640

641

642

643 Julija Zotova: Conceptualization, Methodology, Formal analysis, Investigation, Writing - Original
644 Draft, Visualization.

645 Zaneta Wojnarowska: Conceptualization, Methodology, Formal analysis, Investigation.

646 Brendan Twamley: Methodology, Formal analysis, Investigation, Resources, Writing - Original Draft,
647 Visualization.

648 Lidia Tajber: Conceptualization, Methodology, Formal analysis, Investigation, Resources, Writing -
649 Review & Editing, Visualization, Supervision, Project administration, Funding acquisition.

650 **Declaration of interests**

651

652 ☒ The authors declare that they have no known competing financial interests or personal
653 relationships that could have appeared to influence the work reported in this paper.

654

655 ☐The authors declare the following financial interests/personal relationships which may be
656 considered as potential competing interests:
657

658
659
660

661

662